

# Where to find lossless metals?

Xiaolei Hu,<sup>1,2</sup> Zhengran Wu,<sup>1,2</sup> Zhilin Li,<sup>1,3,\*</sup> Qiunan Xu,<sup>4</sup> Kun Chen,<sup>1,2</sup> Kui Jin,<sup>1,3</sup> Hongming Weng,<sup>1,3,†</sup> and Ling Lu<sup>1,3,‡</sup>

<sup>1</sup>*Institute of Physics, Chinese Academy of Sciences/Beijing National Laboratory for Condensed Matter Physics, Beijing 100190, China.*

<sup>2</sup>*School of Physical Sciences, University of Chinese Academy of Sciences, Beijing 100049, China.*

<sup>3</sup>*Songshan Lake Materials Laboratory, Dongguan, Guangdong 523808, China.*

<sup>4</sup>*Qingdao Institute for Theoretical and Computational Sciences, Shandong University, Qingdao 266237, China.*

Hypothetical metals having optical absorption losses as low as those of the transparent insulators, if found, could revolutionize optoelectronics. We perform the first high-throughput search for lossless metals among all known inorganic materials in the databases of over 100,000 entries. The 381 candidates are identified — having well-isolated partially-filled bands — and are analyzed by defining the figures of merit and classifying their real-space conductive connectivity. The existing experimental evidence of most candidates being insulating, instead of conducting, is due to the limitation of current density functional theory in predicting narrow-band metals that are unstable against magnetism, structural distortion, or electron-electron interactions. We propose future research directions including conductive oxides, intercalating layered materials, and compressing these false-metal candidates under high pressures into eventual lossless metals.

## I. INTRODUCTION

Optical photons and electrons, the most important carriers for information and energy, have never been guided efficiently inside the same material due to the high absorption loss of metals. Dielectrics transport photons as in optical fibers and metals conduct electrons as in copper wires. At the photon energy much above that of the lattice phonons, the optical absorption is dominated by the electronic transitions (direct or indirect) between the occupied and empty states. For all existing metals, at any optical frequency, there are always occupied and empty states available for the absorption process to take place (Fig. 1a), causing the common misimpression that metals have to be lossy due to the so called free-carrier absorption.

Fortunately, the carriers in solids are never free electrons, since their density of states (DOS) can be highly modified by the lattice potentials. It is indeed theoretically possible [1, 2] for a metal to have zero single-electron transition rate in an energy bandwidth in which the photon absorption can be as low as that in insulators (Fig. 1b). This happens when there is a well-isolated metallic band (of band width  $W$  as in Fig. 1c) at the Fermi level with a lossless bandwidth of

$$\hbar\Delta\omega = \min\{G_c, G_v\} - W > 0. \quad (1)$$

Eq. 1 is the lossless criteria in which the band separation, minimal values of  $G_c, G_v$ , have to be larger than  $W$ .  $G_c, G_v$  are the energy differences from the Fermi level to the edges of conduction and valence bands. Here, *lossless* means the absence of single-electron absorption

— the same sense that insulators are considered lossless below the bandgap where the imaginary part of the dielectric constant ( $\epsilon_1 + i\epsilon_2$ ) vanishes ( $\epsilon_2 = 0$ ). Higher order processes, involving multiple electrons, multiple phonons and multiple photons, have much lower probabilities and are neglected. This picture of lossless metals was proposed by Medvedeva and Freeman [1] in the context of ideal transparent conductors and by Khurgin and Sun [2] in the context of ideal plasmonic metamaterials. Although electrified [1] and 2D metals [3] have been suggested as possible directions, lossless metals remain elusive.

The scientific and technological impact of lossless metal is far-reaching. For transparent electronics [1, 4, 5], the inevitable trade-off between conductivity and transmissivity could be broken. For plasmonics [2, 3, 6] ( $\epsilon_1 < 0$ ), optical devices could be losslessly shrunk to deep subwavelength scales, enhancing light-matter interactions at unprecedented level [7]. For metamaterials [2, 3, 6], the numerous remarkable scientific demonstrations, such as cloaking and perfect lens, may deliver practical applications. In reality, even if  $\epsilon_1$  is positive and  $\Delta\omega$  is narrow, lossless metals still have exciting consequences, such as the waveguiding both electricity and light! We notice that the three-band configuration of lossless metals is similar to, although having very different requirements, that of the intermediate-band materials [8], a class of compounds expected to increase the solar-cell efficiency by absorbing a wider spectrum. The field of intermediate-band solar cells also lacks candidate materials [9].

In the rest of the paper, we first introduce the joint-density-of-states (JDOS) picture [3] for understanding lossless metals. Then, a large-scale computational search is performed to find all potential candidates within the framework of the band theory. The candidates are ranked by the figures of merits ( $W$  and  $\Delta\omega$ ) and classified into three classes for their potential conduction paths in the

\* lizhilin@iphy.ac.cn

† hmweng@iphy.ac.cn

‡ linglu@iphy.ac.cn

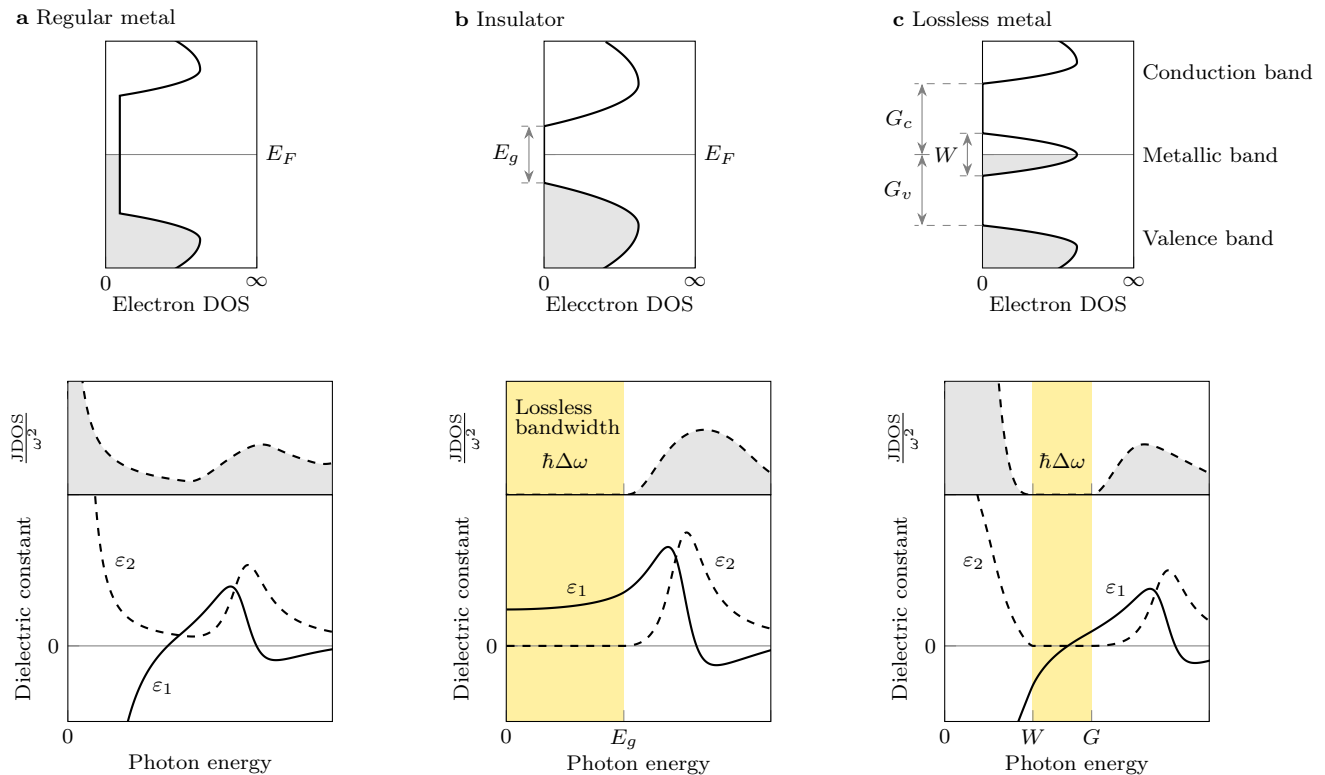


Fig. 1. **Comparison between lossless metal, regular metal and insulator.** **a**, Regular metal is lossy across the whole bandwidth. **b**, Insulator is lossless below the bandgap ( $E_g$ ). **c**, Lossless metal, satisfying the loss criteria ( $W < G = \min\{G_c, G_v\}$ ), have a lossless bandwidth  $\hbar\Delta\omega$  from  $W$  to  $G$ .

real space. After compiling the previous experimental data on the candidate materials, we explain the deficiency of current theory in predicting lossless metals and discuss the next research agenda.

## II. JDOS MODEL OF ABSORPTION

The dielectric constant ( $\varepsilon_2 = 0$ ) of a lossless metal cannot be described by the regular Drude model, whose intra-band absorption is  $\varepsilon_2^{\text{intra}}(\omega) = \frac{\omega_p^2 \Gamma}{\omega(\omega^2 + \Gamma^2)}$ , where  $\omega_p$  is the plasma frequency and  $\Gamma$  is the constant electron scattering rate. It is proposed in Ref. [3] that a frequency-dependant  $\Gamma(\omega) \propto \text{JDOS}(\omega)$ , with JDOS proportionality, correctly gives  $\varepsilon_2 = 0$  inside the lossless bandwidth. The scattering rate is roughly proportional to the JDOS of electrons, because the JDOS captures the phase space of the initial and final states. Here,  $\text{JDOS}(\omega) = \int_0^\omega \text{DOS}(\omega' - \omega) \text{DOS}(\omega') d\omega'$  relaxes the momentum conservation to account for the indirect transitions.

Our JDOS-Drude intra-band model is

$$\Gamma(\omega) = \frac{\text{JDOS}(\omega)}{\omega \cdot \text{DOS}^2(E_F)} \Gamma_{\text{dc}}, \quad (2)$$

where  $\text{DOS}(E_F)$  is the DOS at Fermi energy. At zero frequency,  $\Gamma(0) = \Gamma_{\text{dc}} = \epsilon_0 \frac{\omega_p^2}{4\pi} \rho_{\text{dc}}$  ( $\sim 30\text{THz}$  in silver), in which  $\rho_{\text{dc}}$  is the measurable resistivity of direct current (dc) and  $\epsilon_0$  is the vacuum permittivity. Compared to that in Ref. [3], there is no fitting parameter in our model.

We find that  $\varepsilon_2 \propto \text{JDOS}/\omega^2$  can be used as a qualitative estimation of material absorption (as shown in Fig. 1) for both intra- and inter-band losses. At low frequencies, the intra-band loss dominates and  $\varepsilon_2^{\text{intra}}(\omega \ll \Gamma_{\text{dc}}) = \frac{\omega_p^2}{\Gamma_{\text{dc}} \text{DOS}^2(E_F)} \text{JDOS}/\omega^2$ . At high frequencies, the inter-band loss dominates and the  $\varepsilon_2^{\text{inter}} \propto \text{JDOS}/\omega^2$  scaling is still valid. Since the transition rate, in Fermi's golden rule, is proportional to the vector potential squared  $A^2 = (E/\omega)^2$ , where  $E$  is the electric field [10]. Since the band theory only works in the single-particle regime, it is beneficial to formulate everything using DOS and JDOS that are valid for both interacting and non-interacting electron systems. Equivalently, lossless means zero JDOS.

## III. HIGH-THROUGHPUT SEARCH

We search for lossless metals in two computational online material databases of Materials

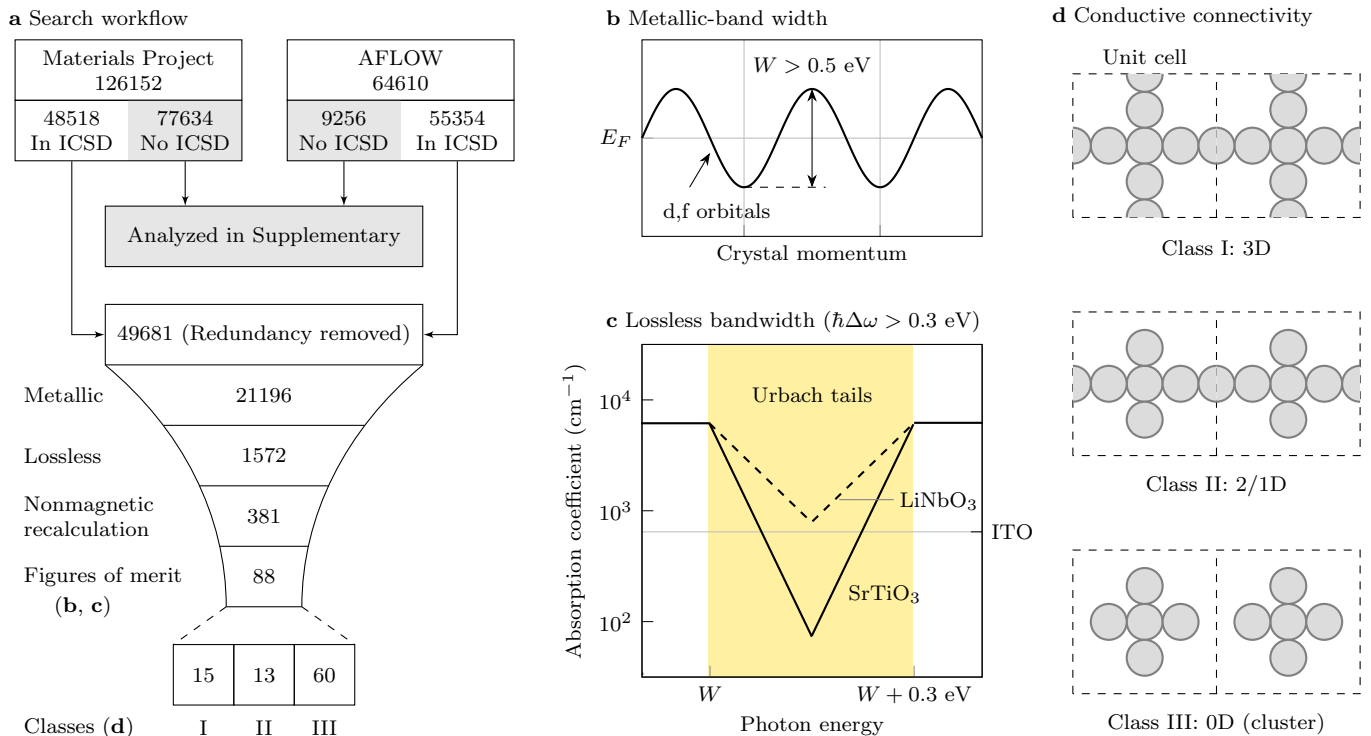


Fig. 2. **The search workflow and analysis of lossless-metal candidates.** **a**, Workflow diagram of the screening steps. **b**, First figure of merit: the metallic-band width containing d/f orbitals. **c**, Second figure of merit: the lossless bandwidth constrained by Urbach absorption tails. **d**, The 88 candidates are classified by their real-space conductive connectivity, whether the relevant atoms are close enough for current flow.

Project (<https://materialsproject.org>) and AFLOW (<http://aflow.org>) with a total of 190762 material entries (in September 2020), shown in Fig.2a. In the main-text, we analyze the materials that have experimental relevance — those listed in the Inorganic Crystal Structure Database (ICSD: <https://icsd.fiz-karlsruhe.de>), a comprehensive collection of experimental crystal data. The rest of the materials, not listed in ICSD, are analyzed in the Appendix B. Among the 92153 ICSD IDs covered in the two databases, there are 49681 unique compounds after we merge the redundant entries of identical stoichiometries and space groups. The band-structure data are available for 42729 compounds and 21196 of them are metals — having partially-filled metallic bands at the Fermi levels.

Each band structure in the databases represents a ground state, either magnetic or non-magnetic, predicted by the density functional theory (DFT) [4, 11]. For non-magnetic ground states, we can directly apply the lossless criteria of Eq. 1 and the energy limit of the search is up to 10 eV. Among the 14463 nonmagnetic (spin-degenerate) metals, we find 431 lossless-metal candidates. For the rest metals with magnetic ground states (spins splitting), we are actually more concerned about their properties at room temperature (for optical applications) above most magnetic-transition temperatures. In order to estimate their nonmagnetic properties from the available magnetic

band structures while keeping enough potential candidates at this step, we relax the lossless criteria to be one of the spin bands satisfying the lossless criteria and obtain 1141 loss-metal candidates. (791 of them satisfies the lossless criteria unconditionally considering both spins.) This spin-criteria is justified by the fact that magnetism mostly split the two spins in the band structures.

Aiming at applications under room-temperature where most materials lose their magnetic ordering, we perform non-magnetic recalculations for all 1572 candidates (431 non-magnetic plus 1141 magnetic candidates), with improved accuracy, to double-check whether they still satisfy the lossless criteria. The high-throughput computations in the databases have compromised settings for speed, while we include the spin-orbit coupling, f-orbitals, as well as experimental lattice data from ICSD. Our ab-initio recalculations are performed using the Vienna Ab initio Simulation Package (VASP) with the generalized gradient approximation (GGA) plus Coulomb repulsion ( $U$ ), detailed in the Appendix A.

First, we drop the 306 candidates whose chemical formula is in fact different from their ICSD entries. They miss hydrogen atoms in the calculations due to the lack of the hydrogen positions in ICSD. Second, we drop 242 candidates whose DFT calculations do not converge, mostly due to the inclusion of the f-orbitals from rare earth elements such as Terbium (Tb) and Ytter-

bium (Yb). Third, in the remaining 1024 candidates with correct composition and converging band structures, 637 candidates no longer satisfy the lossless criteria. Our recalculation is more restrictive for two major reasons. On one hand, the magnetic candidates, from the previous screening step, are not necessarily lossless for their nonmagnetic band structures. On the other hand, the database band structures are based on the computationally-relaxed structures (with GGA DFT), which usually converge to larger lattice constants than the experimental values. An expanded lattice leads to flatter bands so the lossless criteria is easier to be met with the relaxed structures compared to the experimental structures. After all, we have 381 lossless-metal candidates left after the nonmagnetic recalculations.

#### IV. FIGURES OF MERIT

The metallic-band width ( $W$ ) and lossless bandwidth ( $\hbar\Delta\omega$ ) are the two figures of merit for lossless metals. Larger  $W$  usually implies higher mobility and better conductors while larger  $\hbar\Delta\omega$  means lower optical absorption.

We remove candidates whose metallic-band width ( $W$ ) is too narrow to be metals in reality (Fig. 2b). It is well known that a narrow electronic band at Fermi level results in correlation effects (low kinetic energy compared to Coulomb repulsion  $U$ ) that DFT has a limited predictive power. For example,  $W < U$  is considered a condition for Mott insulators, where the  $U$  values are mentioned in Appendix A. This is especially true for d/f orbitals that are intrinsically narrow-banded and spatially localized. Sadly, the lossless metal falls right into this category, because a narrow metallic band is required to satisfy the lossless criteria and 355 of the 381 candidates contain d/f orbitals (from transition-metal elements) in their isolated metallic bands. Consequently, we set an empirical lower limit of 0.5 eV on the metallic-band width and remove 229 candidates whose metallic bands are made of d/f electrons and, at the same time,  $W < 0.5$  eV. We do not constrain s/p orbitals which are usually handled well by DFT. It is worth-noting that, in the case when the metallic band ( $W$ ) consists of several individually isolated sub-bands, only the bandwidth of the partially-filled isolated sub-bands are used as the figure of merit.

We also remove candidates whose lossless bandwidth ( $\hbar\Delta\omega$ ) is too narrow to support low optical absorption in reality (Fig. 2c). Although the electron DOS vanishes abruptly at the band edge in a perfectly periodic crystal, real crystals are imperfect and it is well known that the absorption edge drops exponentially with photon energy — the Urbach tails [13, 14]. The slope of the tail, reflecting crystal disorder, is quantified by the Urbach energy — a temperature-dependent energy scale across which the absorption coefficient drops by 1/e. In Fig. 2c, the room-temperature Urbach energies

of two ternary compounds, 34 meV in SrTiO<sub>3</sub> [15] and 78 meV in LiNbO<sub>3</sub> [16], are used to estimate the minimum lossless bandwidth needed to achieve a low enough absorption loss. We do not use the smallest Urbach energies ( $\sim 10$ meV) in Si and GaAs, because most other materials could not be grown with such high crystalline qualities. We find that  $\hbar\Delta\omega > 0.3$  eV is necessary to realize a lower absorption coefficient than that of the indium tin oxide (ITO [17]), the standard transparent conductor. The 0.3 eV lower bound removes 113 candidates (out of 381), including the LiTi<sub>2</sub>O<sub>4</sub> — a novel transparent superconductor discussed in the later section.

#### V. REAL-SPACE ANALYSIS

88 candidates are left with reasonably wide metallic-band width ( $W$ ) and lossless bandwidth ( $\hbar\Delta\omega$ ). Theoretically, a large  $\hbar\Delta\omega$  ensures optical transparency, but a wide  $W$  cannot always ensure electrical conduction. Because conduction depends more on the real-space wavefunctions than the reciprocal-space band dispersions. For example, localized unpaired electrons cannot flow in the lattice, but they appear as “metals” (partially-filled bands across Fermi level) in the band theory (assuming global Bloch modes across the crystal). So we study whether the conductive atoms — the atoms contributing to the electron DOS at the Fermi level ( $\pm 50$  meV) — are closely-spaced enough to connect a current path in the crystal. The connectivity of these conductive atoms is determined by the spatial overlap of their atomic radii [18]. Illustrated in Fig. 2d, the *conductive connectivity* can be three dimensional (3D), low-dimensional (2D, 1D), or in isolated clusters (0D), according to which we classify the 88 candidates into three classes with 15, 13, and 60 materials, respectively. The candidates of class I, II and most candidates of class III are tabulated in Table I.

The materials in Class I have 3D conductive connectivity (for potential current paths) in vertex-sharing or edge-sharing polyhedrons. The narrow metallic band originates from the localized d/f orbitals. The isolation of the metallic bands is partly due to the large and uniform splitting of the d/f bands in the crystal fields of high symmetries (high space groups). A typical material example is pyrochlore molybdate (Nd<sub>2</sub>Mo<sub>2</sub>O<sub>7</sub>) shown in Fig. 3a, that is experimentally verified to be a metal (resistance decreases with the decrease of temperature) and is a ferromagnet below the Curie temperature of  $\sim 90$ K [22, 23].

The materials in Class II have low-dimensional conductive connectivity, in which the atoms connect more closely in one or two dimensions. The weaker coupling in certain directions facilitates bands of less dispersions and narrower bandwidths [3]. A typical example is calcium nickelate CaNi<sub>4</sub>O<sub>8</sub> in Fig. 3b. Nickel dioxide (NiO<sub>2</sub>) is a layered insulator having an isolated narrow conduction band (see Appendix C). Calcium intercalation, in NiO<sub>2</sub>, supplies itinerant electrons and raises the Fermi level into the middle of this narrow conduction band, thus satis-

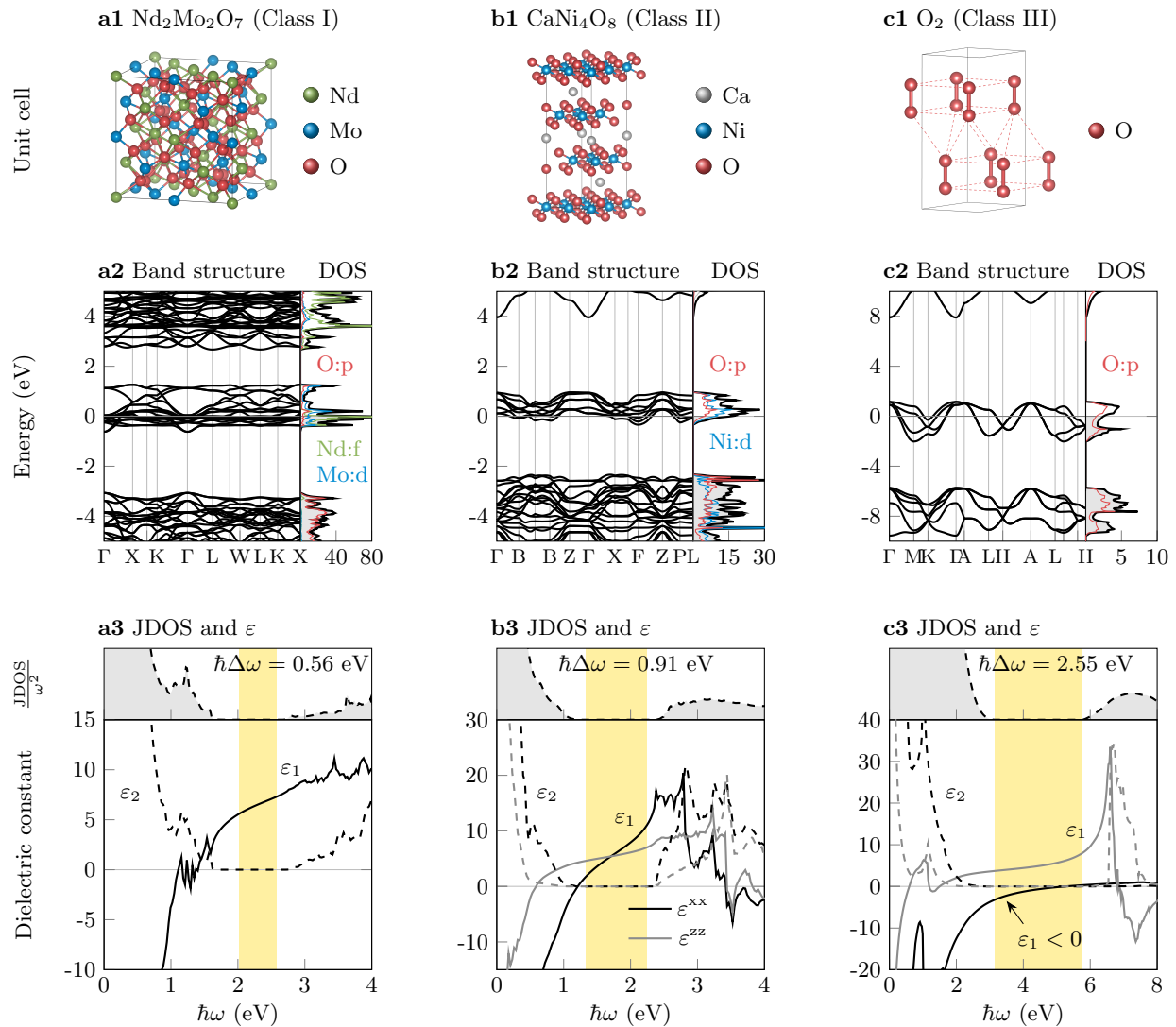


Fig. 3. **Three examples of lossless-metal candidates.** **a1-a3**,  $\text{Nd}_2\text{Mo}_2\text{O}_7$  ( $\text{Fd}\bar{3}\text{m}$ ). **b1-b3**,  $\text{CaNi}_4\text{O}_8$  ( $\text{Fd}\bar{3}\text{m}$ ). **c1-c3**,  $\text{O}_2$  ( $\text{P64}/\text{mmc}$ ). For each material, we plot the crystal structure, band structure, density of states, joint density of states, and dielectric constants. The atomic orbitals constitute the metallic bands are labeled in **a2-c2**. Data of the rest candidates are plotted in the Appendix.

fying the lossless-metal criteria. The same mechanism applies to  $\text{KSnS}_2$  (detailed in Appendix C), in which Potassium intercalates into the tin disulfide ( $\text{SnS}_2$ ) — a common layered material. Neither  $\text{CaNi}_4\text{O}_8$  [39] nor  $\text{KSnS}_2$  [61] have been synthesized in single-crystal forms.

The materials in Class III consist of distanced atomic clusters (forming narrow metallic bands), which are easier, than the other two classes, to satisfy the lossless criteria in DFT calculations. However, the weak couplings between the clusters impede electric conduction. A typical example is the solid oxygen  $\text{O}_2$  ( $\text{P64}/\text{mmc}$ ) in Fig. 3c, showing a huge lossless bandwidth of  $\hbar\Delta\omega = 2.55$  eV with an isolated metallic-band width of  $W = 3.17$  eV. This molecular crystal consists of dense arrangement of diatomic molecules under high pressure. In experiments,

this phase forms at  $\sim 17$  GPa and is not conducting. The oxygen metallizes under a much higher pressure around 100 GPa [8, 24] (see Appendix C for the  $\text{O}_2$  phase diagram).

## VI. EXISTING EXPERIMENTS

We go through the existing experimental literature on the candidates in Table I and note their key feedback information (the references are listed in Appendix C). The cold truth is that, experimentally, most candidates are false metals and real insulators [25], except  $\text{Nd}_2\text{Mo}_2\text{O}_7$  (and the  $\text{LiTi}_2\text{O}_4$  discussed in the next section). The false positive prediction of metals is a common problem

TABLE I: **Lossless-metal candidates.** Top candidates are given for each class, sorted by the lossless bandwidth ( $\hbar\Delta\omega$ ). The experiment references of each material are provided in the Appendix D.

	Formula	Space group	$W$ (eV)	$\hbar\Delta\omega$ (eV)	Conductive connectivity	Magnetism ( $T_C/T_N$ ) distortion	Color	Conduction
Class I	CoCO <sub>3</sub>	167	0.61	1.95	3D	AFM (18K)		Insulator
	K <sub>5</sub> CeCo <sub>2</sub> (NO <sub>2</sub> ) <sub>12</sub>	201	0.85	1.70	3D			
	Ba <sub>2</sub> CoMoO <sub>6</sub>	225	1.12	1.32	3D	AFM (20K)	Black	
	Sr <sub>2</sub> CoMoO <sub>6</sub>	225	1.30	1.24	3D	AFM (36K)	Black	Insulator
	NiMoO <sub>4</sub>	12	0.71	0.91	3D	FM (22K)	Light green	
	Ba <sub>2</sub> GdMoO <sub>6</sub>	225	0.93	0.88	3D		Black	Insulator
	KCoF <sub>3</sub>	221	1.67	0.80	3D	AFM (114K)	Rosy	Insulator
	Nd <sub>2</sub> Mo <sub>2</sub> O <sub>7</sub>	227	2.02	0.59	3D	FM (90K)	Black	Metal
	CoTiO <sub>3</sub>	148	0.74	0.44	3D	AFM (38K)	Green	Insulator
	CaCr <sub>2</sub> O <sub>4</sub>	62	1.69	0.42	3D	AFM (43K)		Insulator
	CaCu <sub>3</sub> Ti <sub>4</sub> O <sub>12</sub>	204	0.89	0.40	3D	AFM (24K)		Insulator
	CuSiO <sub>3</sub>	148	1.13	0.37	3D	AFM (110K)	Black	Insulator
	Li <sub>2</sub> IrO <sub>3</sub>	70	2.75	0.36	3D	FM (38K)		Insulator
	Bi <sub>2</sub> Cu <sub>5</sub> B <sub>4</sub> O <sub>14</sub>	1	0.90	0.35	3D	FM (25K)	Green	Insulator
	NiF <sub>2</sub>	58	1.67	0.30	3D	AFM (73K)		Insulator
LiTi <sub>2</sub> O <sub>4</sub>	227	2.37	0.12	3D	Superconductor (13.7K)	Blue	Metal	
Class II	CaNi <sub>4</sub> O <sub>8</sub>	166	1.33	0.91	2D			
	Sc <sub>2</sub> Cu <sub>2</sub> O <sub>5</sub>	33	0.61	0.80	1D	AFM (16K)		Insulator
	VCl <sub>3</sub>	148	1.19	0.66	2D	FM	Violet	Insulator
	CuZrTiO <sub>5</sub>	19	0.94	0.55	1D	AFM	Green	Insulator
	CuInOPO <sub>4</sub>	62	0.69	0.51	1D		Green	
	Li <sub>2</sub> CuO <sub>2</sub>	71	1.13	0.48	1D	AFM (9K)	Brown	Insulator
	BaCu <sub>2</sub> Si <sub>2</sub> O <sub>7</sub>	62	0.95	0.42	1D	AFM (9.2K)	Dark blue	Insulator
	Co <sub>2</sub> B <sub>2</sub> O <sub>5</sub>	2	1.55	0.41	1D	AFM (45K)	Violet	
	Ca <sub>3</sub> Cu <sub>5</sub> Si <sub>9</sub> O <sub>26</sub>	15	0.96	0.38	2D		Bluish-green	Insulator
	CsNiBr <sub>3</sub>	194	1.14	0.37	1D	AFM (70K)	Orange-brown	
	CaCuGe <sub>2</sub> O <sub>6</sub>	14	0.58	0.36	1D	AFM, Jahn-Teller		Insulator
	Cu(OH)F	14	1.75	0.36	2D	AFM, Jahn-Teller		
	KSnS <sub>2</sub>	166	1.14	0.36	2D			
Class III	NaO <sub>2</sub>	205	0.71	3.57	0D	AFM (193K)		Insulator
	O <sub>2</sub>	194	3.17	2.55	0D	High-pressure	Dark red	Insulator
	Rb <sub>4</sub> O <sub>6</sub>	220	0.42	2.44	0D	AFM	Black	Insulator
	LiO <sub>2</sub>	58	1.84	2.28	0D	AFM (7K)		Insulator
	K <sub>2</sub> BaCo(NO <sub>2</sub> ) <sub>6</sub>	69	1.14	1.61	0D	Jahn-Teller		Insulator
	Nb <sub>2</sub> (PO <sub>4</sub> ) <sub>3</sub>	167	1.16	1.52	0D		Black	Insulator
	Rb <sub>2</sub> NbCl <sub>6</sub>	225	0.71	1.52	0D	Jahn-Teller		
	RbSb	216	0.96	1.27	0D			Insulator
	K <sub>2</sub> TaCl <sub>6</sub>	225	0.98	1.03	0D	Jahn-Teller	Black	Insulator
	K <sub>3</sub> Na(RuO <sub>4</sub> ) <sub>2</sub>	15	0.59	0.97	0D	AFM (70K)	Black	Insulator
	LiBa <sub>2</sub> Cu <sub>3</sub> O <sub>6</sub>	69	0.56	0.96	0D	Jahn-Teller		
	Sr <sub>2</sub> CoWO <sub>6</sub>	225	1.65	0.77	0D	AFM (24K)	Dark brown	Insulator
	Ba <sub>2</sub> MgReO <sub>6</sub>	225	1.50	0.75	0D	AFM	Black blue	Insulator
	KRuO <sub>4</sub>	88	0.78	0.74	0D	AFM (150K)	Black	Insulator
	Cu(HCOO) <sub>2</sub>	14	0.97	0.69	0D	AFM (17K)	Light blue	Insulator
	SrCu <sub>2</sub> (BO <sub>3</sub> ) <sub>2</sub>	140	0.99	0.59	0D	AFM (1.4K)	Blue	Insulator
	CuSe <sub>2</sub> O <sub>5</sub>	15	0.84	0.48	0D	AFM	Green	Insulator
	Ba <sub>2</sub> CoWO <sub>6</sub>	225	1.93	0.44	0D	AFM (17K)	Brown	Insulator

$T_C/T_N$ : Curie/Neel temperature of magnetic transition. FM: ferromagnetism. AFM: antiferromagnetism.

of DFT for complex materials involving transition-metal elements, d/f electrons, narrow bands, magnetism, or correlation effects. In reality, these materials usually find insulating ground states of lower energies, than the predicted metallic states, by structure distortions, magnetic orderings, or electron-electron interactions. As can be seen in Table I, magnetism and cooperative Jahn-Teller distortion are observed for most candidates.

Magnetic orders are difficult to predict. Even the para-magnetic states above the temperatures of magnetic phase transitions, containing disordered local magnetic moments, remains a challenge for DFT [25]. So far, our recalculations are nonmagnetic, assuming zero local magnetic moments. The above facts cast doubts on whether more candidates would turn out to be true metals or whether the electronic state of  $\text{Nd}_2\text{Mo}_2\text{O}_7$  (Fig. 3a) is predicted accurately enough to satisfy the lossless criteria in experiments.

Optical loss is a property not having much data in the literature. In most reports, only the sample color is mentioned. But we do require the broad-band dielectric constants  $\varepsilon(\omega)$ , using tools such as the ellipsometry or transmission/reflection, to verify the predictions. Note that the optical absorption ( $\varepsilon_2$ ) is sensitive to the sample quality, so low loss is generally harder to verify experimentally than electric conduction.

## VII. THE CASE OF $\text{LiTi}_2\text{O}_4$

One positive prediction of our search is lithium titanate  $\text{LiTi}_2\text{O}_4$  (Fd $\bar{3}m$ ), a well studied metal having a superconducting ground state [37], rather than the magnetic orders or Jahn-Teller distortions observed for the false-metal candidates or the magnetic metal  $\text{Nd}_2\text{Mo}_2\text{O}_7$  in Table I. Thin-film  $\text{LiTi}_2\text{O}_4$  is transparent [38] with a reasonably low optical loss [28]. Prepared by the pulsed laser deposition, the film deteriorates in air and its quality is usually limited by oxygen vacancies. Bulk single crystals of  $\text{LiTi}_2\text{O}_4$  are difficult to grow [29].

Although the above experimental feedback of  $\text{LiTi}_2\text{O}_4$  agrees with our predictions in Appendix C, its theoretical lossless bandwidth is too narrow ( $\hbar\Delta\omega = 0.12$  eV) to support an optical absorption much lower than that of ITO. Nevertheless, it is encouraging to find that realistic metal satisfying the lossless criteria can exist. A metal of a larger lossless bandwidth awaits identification.

## VIII. FUTURE DIRECTIONS

Although the feedback from existing experiments indicate the drawbacks of the current high-throughput approach in finding lossless metals, the candidates in Table I still serve as reasonable starting points. Efforts should be made to study their failure modes, their actual electronic structures and their optical properties. These efforts involve ab-initio calculations beyond simple DFT [25] such

as the dynamical mean-field theory (DMFT), as well as the experimental attempts in growing and characterizing the high-quality single-crystal samples that most of the candidates lack.

The candidates also indicate promising directions for future searches. Obviously, majority of the entries in Table I are oxides [30]. In Class I, transition-metal compounds with high spatial symmetries are promising material systems, for examples the double perovskites (such as  $\text{Ba}_2\text{CoMoO}_6$ ), pyrochlore ( $\text{Nd}_2\text{Mo}_2\text{O}_7$ ), and spinel ( $\text{LiTi}_2\text{O}_4$ ). In Class II, layered insulators of a narrow band near Fermi level (such as the  $\text{SnS}_2$  and  $\text{NiO}_2$  presented in Appendix C) worth the attention, since their Fermi levels could be tuned by intercalation.

Inspired by the solid oxygen in Class III, we propose a novel high-pressure route to lossless metals. Conceptually, there are two ways to obtain narrow-band metals. One way is expanding the lattice constant of a metal [2] to narrow its bandwidth while maintaining its conduction. However, there is no experimental technique to do that. The other way is shrinking the lattice constant of a false-metal candidate in order to widen its metallic bandwidth into a metal, through an insulator-metal transition, while maintaining a finite lossless bandwidth. The standard high-pressure technique using diamond-anvil cell is well suited for this purpose, since both the transmission/reflection and the resistance can be monitored when the pressure is applied to the sample [31].

## IX. CONCLUSION

We perform the first high-throughput screening for the elusive lossless metals. Starting from 44660 distinctive inorganic materials in ICSD, we obtain 88 high-quality candidates, while most of them are found to be insulating in experiments. Lossless metals are difficult to predict using the current condensed-matter theory due to the complexity of the candidate material systems. Nevertheless, our results shine light on a few hopeful directions including oxide conductors, low-dimensional metals, and compressing the false-metal candidates. Finally, we emphasize that our current search is far from complete, because the data quantity and accuracy in the databases are still under development. The search could also be extended to organic materials [32].

## ACKNOWLEDGMENT

We acknowledge the SC2 group at our institute led by Kui Jin for investigating  $\text{LiTi}_2\text{O}_4$ . This work is supported by the the Chinese Academy of Sciences through the Youth Innovation Promotion Association (2021008), the Project for Young Scientists in Basic Research (YSBR-021), the Strategic Priority Research Program (XDB33000000), the Informatization Plan (CAS-WX2021SF-0102), the Inter-

disciplinary Innovation Team, and the International Partnership Program with the Croucher Foundation (112111KYBS20200024), by the National Key R&D Program of China (2017YFA0303800, 2017YFA0303800,

2018YFA0305700), by Natural Science Foundation of China (12025409, 11721404, 11974415, 12025409, 11721404, 11974415, 11925408, 11921004, 12188101), and by Beijing Natural Science Foundation (Z200008).

- 
- [1] J. E. Medvedeva and A. J. Freeman, “Combining high conductivity with complete optical transparency: A band structure approach,” *EPL (Europhysics Letters)* **69**, 583 (2005).
- [2] J. B. Khurgin and G. Sun, “In search of the elusive lossless metal,” *Applied Physics Letters* **96**, 181102 (2010).
- [3] M. N. Gjerding, M. Pandey, and K. S. Thygesen, “Band structure engineered layered metals for low-loss plasmonics,” *Nature communications* **8**, 15133 (2017).
- [4] Xiuwen Zhang, Lijun Zhang, *et al.*, “Intrinsic transparent conductors without doping,” *Physical review letters* **115**, 176602 (2015).
- [5] G. Brunin, F. Ricci, V. Ha, *et al.*, “Transparent conducting materials discovery using high-throughput computing,” *npj Computational Materials* **5**, 1–13 (2019).
- [6] J. B. Khurgin and A. Boltasseva, “Reflecting upon the losses in plasmonics and metamaterials,” *MRS bulletin* **37**, 768–779 (2012).
- [7] O. D. Miller, A. G. Polymeridis, *et al.*, “Fundamental limits to optical response in absorptive systems,” *Optics express* **24**, 3329–3364 (2016).
- [8] A. Luque and A. Martí, “Increasing the efficiency of ideal solar cells by photon induced transitions at intermediate levels,” *Physical Review Letters* **78**, 5014 (1997).
- [9] D. JR. Baquião and G. M. Dalpian, “Computational screening of bulk materials with intrinsic intermediate band,” *Computational Materials Science* **158**, 382–388 (2019).
- [10] G. Grosso and G. P. Parravicini, *Solid state physics* (Academic press, 2013).
- [11] A. Jain *et al.*, “A high-throughput infrastructure for density functional theory calculations,” *Computational Materials Science* **50**, 2295–2310 (2011).
- [4] S. Curtarolo *et al.*, “AFLOW: an automatic framework for high-throughput materials discovery,” *Computational Materials Science* **58**, 218–226 (2012).
- [13] F. Urbach, “The long-wavelength edge of photographic sensitivity and of the electronic absorption of solids,” *Phys. Rev.* **92**, 1324 (1953).
- [14] S.S. Mitra and B. Bendow, *Optical Properties of Highly Transparent Solids* (Plenum, New York, 1975).
- [15] D Goldschmidt and HL Tuller, “Fundamental absorption edge of SrTiO<sub>3</sub> at high temperatures,” *Physical Review B* **35**, 4360 (1987).
- [16] R. Bhatt *et al.*, “Urbach tail and bandgap analysis in near stoichiometric LiNbO<sub>3</sub> crystals,” *Phys. Status Solidi A* **209**, 176–180 (2012).
- [17] T. AF König *et al.*, “Electrically tunable plasmonic behavior of nanocube–polymer nanomaterials induced by a redox-active electrochromic polymer,” *ACS nano* **8**, 279–287 (2014).
- [18] J. C Slater, “Atomic radii in crystals,” *The Journal of Chemical Physics* **41**, 3199–3204 (1964).
- [22] I. Kézsmárki *et al.*, “Charge dynamics near the electron-correlation induced metal-insulator transition in pyrochlore-type molybdates,” *Physical review letters* **93**, 266401 (2004).
- [23] I. Kézsmárki *et al.*, “Magneto-optical effect induced by spin chirality of the itinerant ferromagnet Nd<sub>2</sub>Mo<sub>2</sub>O<sub>7</sub>,” *Physical Review B* **72**, 094427 (2005).
- [39] PN Bityutskij and VI Khitrova, “Electron diffraction investigation into crystal structures of anhydrous nickelates of alkaline earth elements (Ca, Sr, Ba),” *Kristallografiya* **29**, 450–454 (1984).
- [61] M Bronold, C Pettenkofer, and W Jaegermann, “Alkali metal intercalation into SnS<sub>2</sub>,” *Applied Physics A* **52**, 171–179 (1991).
- [8] Y. Akahama, H. Kawamura, *et al.*, “New high-pressure structural transition of oxygen at 96 GPa associated with metallization in a molecular solid,” *Physical review letters* **74**, 4690 (1995).
- [24] K Shimizu, Eremets MI, K Suhara, and K Amaya, “Oxygen under high pressure-temperature dependence of electrical resistance,” *The Review of High Pressure Science and Technology* **7**, 784–786 (1998).
- [25] O. I Malyi and A. Zunger, “False metals, real insulators, and degenerate gapped metals,” *Applied Physics Reviews* **7**, 041310 (2020).
- [37] D. C. Johnston, H. Prakash, W. H. Zachariasen, and R. Viswanathan, “High temperature superconductivity in the Li-Ti-O ternary system,” *Materials Research Bulletin* **8**, 777–784 (1973).
- [38] A. Kumatani *et al.*, “Growth processes of lithium titanate thin films deposited by using pulsed laser deposition,” *Applied Physics Letters* **101**, 123103 (2012).
- [28] M. Zhao, J. Lian, *et al.*, “Investigation of the optical properties of LiTi<sub>2</sub>O<sub>4</sub> and Li<sub>4</sub>Ti<sub>5</sub>O<sub>12</sub> spinel films by spectroscopic ellipsometry,” *Optical Materials Express* **6**, 3366–3374 (2016).
- [29] C Chen, M Spears, F Wondre, and J Ryan, “Crystal growth and superconductivity of LiTi<sub>2</sub>O<sub>4</sub> and Li<sub>1+1/3</sub>Ti<sub>2-1/3</sub>O<sub>4</sub>,” *Journal of Crystal Growth* **250**, 139–145 (2003).
- [30] N. Tsuda, K. Nasu, A. Fujimori, and K. Siratori, *Electronic conduction in oxides*, Vol. 94 (Springer Science & Business Media, 2000).
- [31] A. Jayaraman, “Diamond anvil cell and high-pressure physical investigations,” *Reviews of Modern Physics* **55**, 65 (1983).
- [32] L. S Xie, G. Skorupskii, and M. Dincă, “Electrically conductive metal–organic frameworks,” *Chemical reviews* **120**, 8536–8580 (2020).

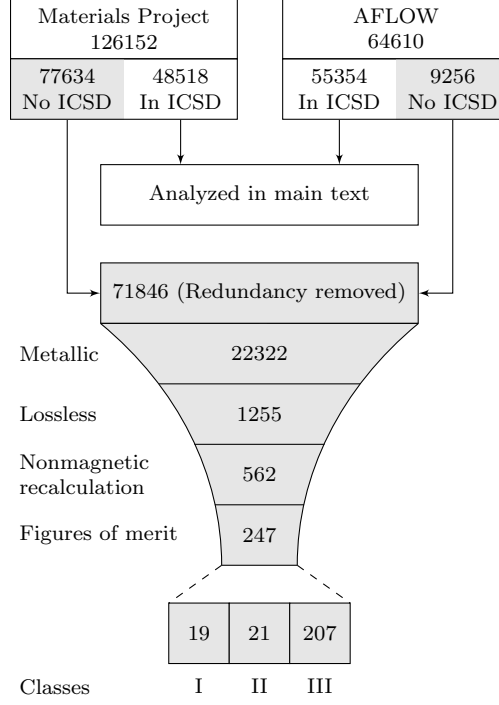


## Appendix A: Settings for first-principle calculations

The calculations in the workflows are performed by VASP [1] with standard generalized gradient approximation (GGA) of the Perdew–Burke–Ernzerhof (PBE)-type exchange-correlation potential [2]. The pseudopotential files that we used are from PAW (projector augmented wave) datasets v.54 in VASP and are selected to be consistent with what are used in both databases (Materials Project and AFLOW). The DFT + U method is based on the simplest rotationally invariant formulation while the values of U are consistent with those used in both databases [3, 4]. The cut-off energy of the plane wave basis set is set to be the ENMAX value in the pseudopotential file plus 25%. A  $\Gamma$ -centered Monkhorst-Pack grid with 40 k-points per  $\text{\AA}^{-3}$  is used for the self-consistent calculations. A doubly dense grid is used for the density-of-states calculations with an energy interval of 5 meV. The k-points files along high symmetry lines for band structure calculations are consistent with the choices in Materials Project. The spin-orbital coupling is included. The optical dielectric constants are computed by WIEN2k [5, 6] using our JDOS model in the maintext.

### Appendix B: Search workflow without ICSD ids

In the main text, we presented the workflow (Fig. 2a) and candidates (Table I and Table sII) from the high-throughput search among materials in ICSD, those have been reported in experiments. Here we present the workflow (Fig. s1) and candidates (Table sI) from the high-throughput search among materials NOT in ICSD, those have NOT been reported in experiments.

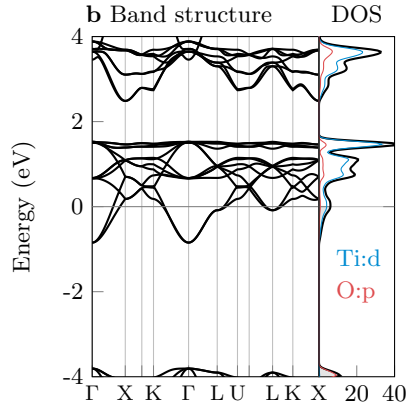
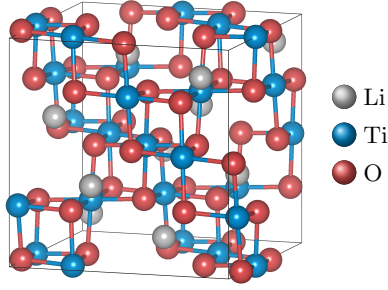
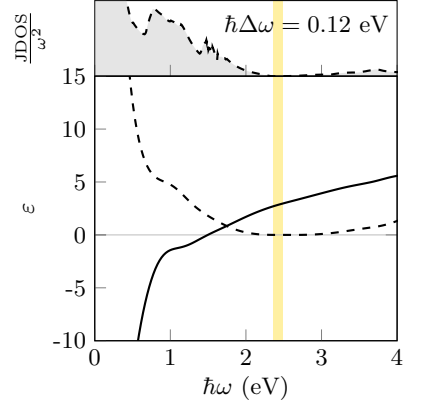


**Fig. S1.** Workflow of the search for lossless metal among materials in the computational database of Material Project and AFlow but not in the experimental database of ICSD.

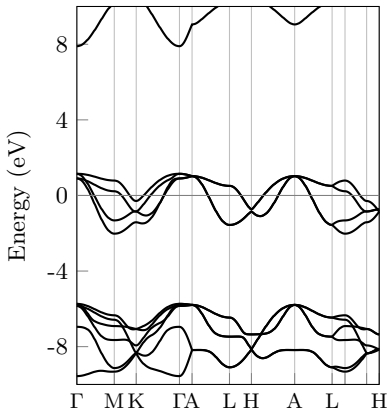
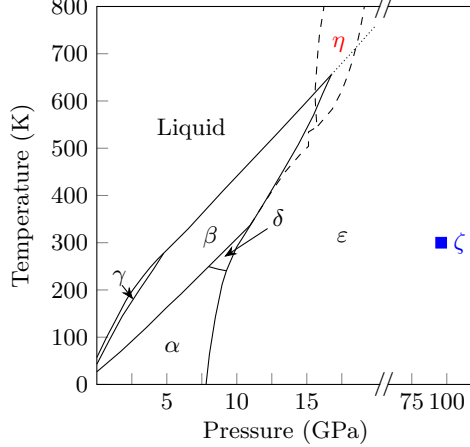
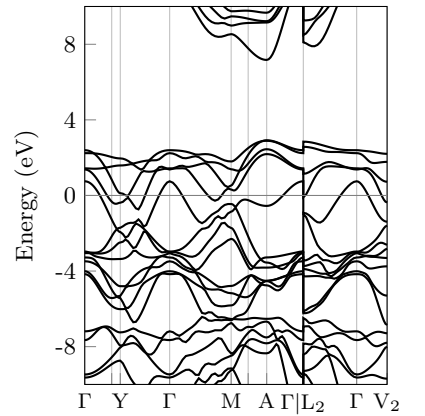
**Table. S1.** Lossless-metal candidates without ICSD IDs. Representative candidates are given for each class, ranked by the lossless bandwidth. The full list are tabulated in the Supplementary Excel file. These materials may not exist.

Class I				Class II				Class III			
Formula	Space group	$W$ (eV)	$\hbar\Delta\omega$ (eV)	Formula	Space group	$W$ (eV)	$\hbar\Delta\omega$ (eV)	Formula	Space group	$W$ (eV)	$\hbar\Delta\omega$ (eV)
YbF <sub>3</sub>	225	4.76	2.81	ZrCoO <sub>3</sub>	148	0.61	0.89	F	194	4.21	7.90
Ba <sub>2</sub> HoMoO <sub>6</sub>	225	1.09	1.00	Li <sub>2</sub> Co <sub>3</sub> TeO <sub>8</sub>	166	1.67	0.83	BaF <sub>3</sub>	139	2.20	5.62
KLuO <sub>3</sub>	221	3.23	0.79	CrF <sub>5</sub>	71	0.78	0.79	RbNaO <sub>3</sub>	221	2.42	4.74
MnNF <sub>3</sub>	62	1.45	0.73	Li <sub>2</sub> CuF <sub>4</sub>	65	0.99	0.77	Cs <sub>2</sub> NaLiF <sub>6</sub>	225	4.50	3.38
CsTbO <sub>3</sub>	221	2.48	0.60	NaMnO <sub>2</sub>	194	1.08	0.64	CaSbF <sub>6</sub>	148	0.58	3.20
Cu <sub>2</sub> OF <sub>2</sub>	141	1.32	0.56	LiTiO <sub>2</sub>	194	1.59	0.58	LiSn(PO <sub>3</sub> ) <sub>4</sub>	60	0.56	2.39
V <sub>2</sub> Si <sub>2</sub> O <sub>7</sub>	227	0.81	0.47	TiCoF <sub>3</sub>	221	1.55	0.46	RbS	123	2.04	2.25
LiAg <sub>2</sub> F <sub>4</sub>	227	0.77	0.40	CuCl <sub>2</sub>	166	0.68	0.45	SbP <sub>2</sub> O <sub>7</sub>	14	0.28	1.68
Na <sub>2</sub> Ni <sub>5</sub> O <sub>10</sub>	2	1.54	0.38	NaNb <sub>2</sub> O <sub>4</sub>	57	1.90	0.38	Li <sub>8</sub> BiO <sub>6</sub>	148	0.65	1.06
SrC <sub>2</sub>	166	5.04	0.37	Ni(OH) <sub>2</sub>	12	0.99	0.34	Ba <sub>2</sub> ScReO <sub>6</sub>	225	1.84	0.44

## Appendix C: More examples

a  $\text{LiTi}_2\text{O}_4$  (Fd-3m)**c** Dielectric constant

**Fig. S2. Class-I lossless metal candidate  $\text{LiTi}_2\text{O}_4$  (space group 227).** The narrow lossless bandwidth of 0.12 eV could be enlarged by pulling down the Fermi level.

**a****b****c**

**Fig. S3. Class-III lossless metal candidate  $\text{O}_2$  ( $\eta$ -phase, space group 194).** **a**,  $\eta$ -phase band structure. **b**, The phase diagram of high-pressed  $\text{O}_2$  [7]. **c**, Structure of metallic  $\zeta$ - $\text{O}_2$  is still unknown. The crystal structure we use here is isomorphic to  $\epsilon$ - $\text{O}_2$  (space group 12) with the lattice parameters:  $a = 3.332 \text{ \AA}$ ,  $b = 4.426 \text{ \AA}$ ,  $c = 6.866 \text{ \AA}$ ,  $\beta = 116.4^\circ$  [8].

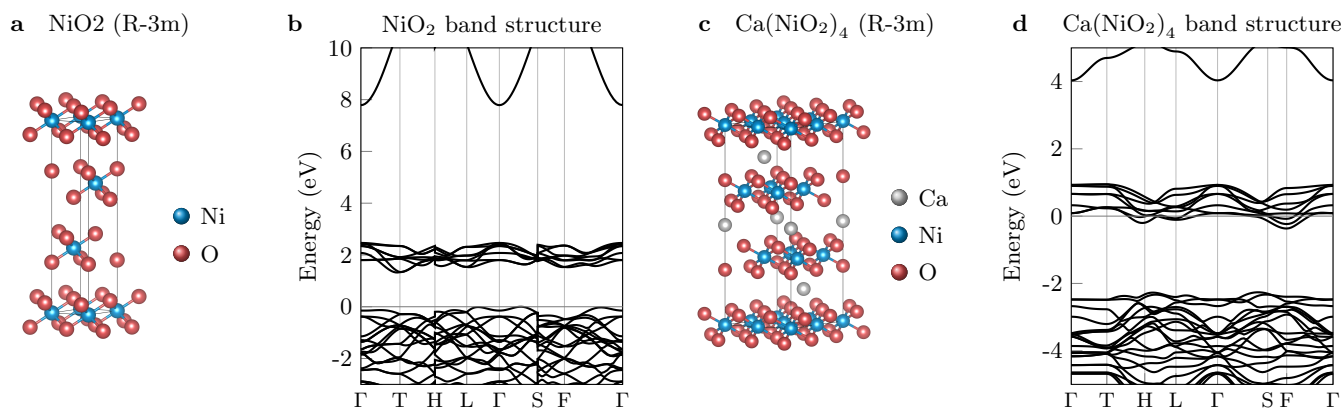


Fig. S 4. Class-II lossless metal candidate  $\text{Ca}(\text{NiO}_2)_4$  (space group 166), compared with  $\text{NiO}_2$  (space group 166).

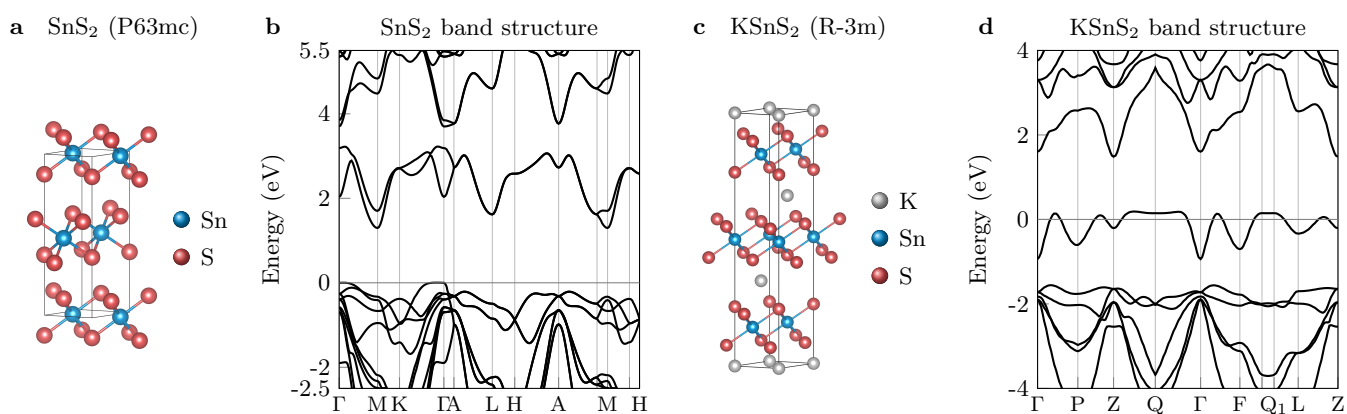


Fig. S 5. Class-II lossless metal candidate  $\text{KSnS}_2$  (space group 166), compared with  $\text{SnS}_2$  (space group 186).

	Formula	Space group	$W$ (eV)	$\hbar\Delta\omega$ (eV)	Conductive connectivity	Magnetism ( $T_C/T_N$ ) distortion	Color	Conduction	Reference
Class I	CoCO <sub>3</sub>	167	0.61	1.95	3D	AFM (18K)		Insulator	[9, 10]
	K <sub>5</sub> CeCo <sub>2</sub> (NO <sub>2</sub> ) <sub>12</sub>	201	0.85	1.70	3D				[11]
	Ba <sub>2</sub> CoMoO <sub>6</sub>	225	1.12	1.32	3D	AFM (20K)	Black		[12, 13]
	Sr <sub>2</sub> CoMoO <sub>6</sub>	225	1.30	1.24	3D	AFM (36K)	Black	Insulator	[14, 15]
	NiMoO <sub>4</sub>	12	0.71	0.91	3D	FM (22K)	Light green		[16]
	Ba <sub>2</sub> GdMoO <sub>6</sub>	225	0.93	0.88	3D		Black	Insulator	[17, 18]
	KCoF <sub>3</sub>	221	1.67	0.80	3D	AFM (114K)	Rosy	Insulator	[19, 20]
	Nd <sub>2</sub> Mo <sub>2</sub> O <sub>7</sub>	227	2.02	0.59	3D	FM (90K)	Black	Metal	[21–23]
	CoTiO <sub>3</sub>	148	0.74	0.44	3D	AFM (38K)	Green	Insulator	[24–26]
	CaCr <sub>2</sub> O <sub>4</sub>	62	1.69	0.42	3D	AFM (43K)		Insulator	[27]
	CaCu <sub>3</sub> Ti <sub>4</sub> O <sub>12</sub>	204	0.89	0.40	3D	AFM (24K)		Insulator	[28–30]
	CuSiO <sub>3</sub>	148	1.13	0.37	3D	AFM (110K)	Black	Insulator	[31]
	Li <sub>2</sub> IrO <sub>3</sub>	70	2.75	0.36	3D	FM (38K)		Insulator	[32]
	Bi <sub>2</sub> Cu <sub>5</sub> B <sub>4</sub> O <sub>14</sub>	1	0.90	0.35	3D	FM (25K)	Green	Insulator	[33, 34]
	NiF <sub>2</sub>	58	1.67	0.30	3D	AFM (73K)		Insulator	[35, 36]
LiTi <sub>2</sub> O <sub>4</sub>	227	2.37	0.12	3D	Superconductor (13.7K)	Blue	Metal	[37, 38]	
Class II	CaNi <sub>4</sub> O <sub>8</sub>	166	1.33	0.91	2D				[39]
	Sc <sub>2</sub> Cu <sub>2</sub> O <sub>5</sub>	33	0.61	0.80	1D	AFM (16K)		Insulator	[40]
	VCl <sub>3</sub>	148	1.19	0.66	2D	FM	Violet	Insulator	[41, 42]
	CuZrTiO <sub>5</sub>	19	0.94	0.55	1D	AFM	Green	Insulator	[43, 44]
	CuInOPO <sub>4</sub>	62	0.69	0.51	1D		Green		[45]
	Li <sub>2</sub> CuO <sub>2</sub>	71	1.13	0.48	1D	AFM (9K)	Brown	Insulator	[46–48]
	BaCu <sub>2</sub> Si <sub>2</sub> O <sub>7</sub>	62	0.95	0.42	1D	AFM (9.2K)	Dark blue	Insulator	[49, 50]
	Co <sub>2</sub> B <sub>2</sub> O <sub>5</sub>	2	1.55	0.41	1D	AFM (45K)	Violet		[51, 52]
	Ca <sub>3</sub> Cu <sub>5</sub> Si <sub>9</sub> O <sub>26</sub>	15	0.96	0.38	2D		Bluish-green	Insulator	[53]
	CsNiBr <sub>3</sub>	194	1.14	0.37	1D	AFM (70K)	Orange-brown		[54, 55]
	CaCuGe <sub>2</sub> O <sub>6</sub>	14	0.58	0.36	1D	AFM, Jahn-Teller		Insulator	[56–58]
Cu(OH)F	14	1.75	0.36	2D	AFM, Jahn-Teller			[59, 60]	
KSnS <sub>2</sub>	166	1.14	0.36	2D				[61]	
Class III	NaO <sub>2</sub>	205	0.71	3.57	0D	AFM (193K)		Insulator	[62, 63]
	O <sub>2</sub>	194	3.17	2.55	0D	High-pressure	Dark red	Insulator	[7, 64, 65]
	Rb <sub>4</sub> O <sub>6</sub>	220	0.42	2.44	0D	AFM	Black	Insulator	[66, 67]
	LiO <sub>2</sub>	58	1.84	2.28	0D	AFM (7K)		Insulator	[68, 69]
	K <sub>2</sub> BaCo(NO <sub>2</sub> ) <sub>6</sub>	69	1.14	1.61	0D	Jahn-Teller		Insulator	[70–72]
	Nb <sub>2</sub> (PO <sub>4</sub> ) <sub>3</sub>	167	1.16	1.52	0D		Black	Insulator	[73]
	Rb <sub>2</sub> NbCl <sub>6</sub>	225	0.71	1.52	0D	Jahn-Teller			[74]
	RbSb	216	0.96	1.27	0D			Insulator	[75]
	K <sub>2</sub> TaCl <sub>6</sub>	225	0.98	1.03	0D	Jahn-Teller	Black	Insulator	[76, 77]
	K <sub>3</sub> Na(RuO <sub>4</sub> ) <sub>2</sub>	15	0.59	0.97	0D	AFM (70K)	Black	Insulator	[78]
	LiBa <sub>2</sub> Cu <sub>3</sub> O <sub>6</sub>	69	0.56	0.96	0D	Jahn-Teller			[79]
	Sr <sub>2</sub> CoWO <sub>6</sub>	225	1.65	0.77	0D	AFM (24K)	Dark brown	Insulator	[80]
	Ba <sub>2</sub> MgReO <sub>6</sub>	225	1.50	0.75	0D	AFM	Black blue	Insulator	[81, 82]
	KRuO <sub>4</sub>	88	0.78	0.74	0D	AFM (150K)	Black	Insulator	[83]
	Cu(HCOO) <sub>2</sub>	14	0.97	0.69	0D	AFM (17K)	Light blue	Insulator	[84, 85]
	SrCu <sub>2</sub> (BO <sub>3</sub> ) <sub>2</sub>	140	0.99	0.59	0D	AFM (1.4K)	Blue	Insulator	[86, 87]
	CuSe <sub>2</sub> O <sub>5</sub>	15	0.84	0.48	0D	AFM	Green	Insulator	[88]
Ba <sub>2</sub> CoWO <sub>6</sub>	225	1.93	0.44	0D	AFM (17K)	Brown	Insulator	[89]	

$T_C/T_N$ : Curie/Neel temperature of magnetic transition. FM: ferromagnetism. AFM: antiferromagnetism.

**Table. S II. Lossless-metal candidates in ICSD with experimental references.** The band structures and dielectric constants of the candidates are appended at the end of this Supplementary Material.

- 
- [1] G. Kresse and J. Furthmüller, Efficient iterative schemes for ab initio total-energy calculations using a plane-wave basis set, *Physical review B* **54**, 11169 (1996).
- [2] J. P. Perdew, K. Burke, and M. Ernzerhof, Generalized gradient approximation made simple, *Physical review letters* **77**, 3865 (1996).
- [3] S. Dudarev, G. Botton, *et al.*, Electron-energy-loss spectra and the structural stability of nickel oxide: An LSDA+U study, *Physical Review B* **57**, 1505 (1998).
- [4] S. Curtarolo *et al.*, AFLOW: an automatic framework for high-throughput materials discovery, *Computational Materials Science* **58**, 218 (2012).
- [5] P. Blaha *et al.*, WIEN2k, an augmented plane wave plus local orbitals program for calculating crystal properties, Vienna University of Technology, Vienna, Austria (2001).
- [6] C. Ambrosch-Draxl and J. O. Sofo, Linear optical properties of solids within the full-potential linearized augmented planewave method, *Computer physics communications* **175**, 1 (2006).
- [7] L. F. Lundegaard, C. Guillaume, *et al.*, On the structure of high-pressure high-temperature  $\eta$ -O<sub>2</sub>, *The Journal of chemical physics* **130**, 164516 (2009).
- [8] Y. Akahama, H. Kawamura, *et al.*, New high-pressure structural transition of oxygen at 96 GPa associated with metalization in a molecular solid, *Physical review letters* **74**, 4690 (1995).
- [9] F. Pertlik, Structures of hydrothermally synthesized cobalt (II) carbonate and nickel (II) carbonate, *Acta Crystallographica Section C: Crystal Structure Communications* **42**, 4 (1986).
- [10] V. C. Srivastava, Effect of pressure on the Néel temperature of MnCO<sub>3</sub>, CoCO<sub>3</sub>, and FeCO<sub>3</sub>, *Journal of Applied Physics* **41**, 1190 (1970).
- [11] A. Ferrari, L. Cavalca, and M. Nardelli, Metalloesnitriti di un catione trivalente (ceoy)e di un catione monovalente (K, Rb, Cs, N H4, Tl), *Gazzetta Chimica Italiana* **81**, 964 (1951).
- [12] J.-S. Kang, H. Han, *et al.*, Electronic structure of the double-perovskite Ba<sub>2</sub>FeMoO<sub>6</sub> using photoemission spectroscopy, *Physical Review B* **64**, 024429 (2001).
- [13] M. J. Martínez-Lope, J. A. Alonso, *et al.*, Preparation, crystal and magnetic structure of the double perovskites Ba<sub>2</sub>CoBO<sub>6</sub> (B= Mo, W), *European Journal of Inorganic Chemistry* **2002**, 2463 (2002).
- [14] V. Gagulin, S. Korchagina, V. Ivanova, and Y. A. Shevchuk, Synthesis and properties of Sr<sub>2</sub>CoMoO<sub>6</sub> and Sr<sub>2</sub>NiMoO<sub>6</sub>, *Inorganic materials* **39**, 625 (2003).
- [15] S. A. Ivanov, S. G. Eriksson, *et al.*, The magnetoelectric perovskite Sr<sub>2</sub>CoMoO<sub>6</sub>: An insight from neutron powder diffraction, *Materials research bulletin* **40**, 840 (2005).
- [16] H. Ehrenberg, I. Svoboda, *et al.*, Crystal and magnetic structure of  $\alpha$ -NiMoO<sub>4</sub>, *Journal of magnetism and magnetic materials* **150**, 371 (1995).
- [17] A. McLaughlin, Magnetic and structural studies of the double perovskites Ba<sub>2</sub>REMO<sub>6</sub>, *Solid state communications* **137**, 354 (2006).
- [18] T. K. Wallace, R. H. Colman, and A. C. McLaughlin, A variable temperature synchrotron x-ray diffraction study of the ferroelastic double perovskite Ba<sub>2</sub>GdMoO<sub>6</sub>, *Physical Chemistry Chemical Physics* **15**, 8672 (2013).
- [19] P. Markovin, R. Pisarev, G. Smolensky, and P. Synchronov, Observation of isotropic magnetic contribution to the refractive index of ABF<sub>3</sub>-type cubic crystals, *Solid State Communications* **19**, 185 (1976).
- [20] A. Ratuszna, A. Pietraszko, A. Chelkowski, and K. Lukaszewicz, The temperature dependence of lattice parameters of KMeF<sub>3</sub> and KMn<sub>0.9</sub>Me<sub>0.1</sub>F<sub>3</sub> compounds (Me= Mn<sup>2+</sup>, Co<sup>2+</sup>, and Ni<sup>2+</sup>), *physica status solidi (a)* **54**, 739 (1979).
- [21] Y. Moritomo, S. Xu, *et al.*, Chemical pressure control of exchange interaction in Mo pyrochlore, *Physical Review B* **63**, 144425 (2001).
- [22] I. Kézsmárki, N. Hanasaki, *et al.*, Charge dynamics near the electron-correlation induced metal-insulator transition in pyrochlore-type molybdates, *Physical review letters* **93**, 266401 (2004).
- [23] I. Kézsmárki, S. Onoda, *et al.*, Magneto-optical effect induced by spin chirality of the itinerant ferromagnet Nd<sub>2</sub>Mo<sub>2</sub>O<sub>7</sub>, *Physical Review B* **72**, 094427 (2005).
- [24] R. Newnham, J. Fang, and R. Santoro, Crystal structure and magnetic properties of CoTiO<sub>3</sub>, *Acta Crystallographica* **17**, 240 (1964).
- [25] J. Roset, A. Fernández, X. Obradors, and J. Tejada, Mössbauer emission studies of 57Co-doped ZnO, Cu<sub>2</sub>O, and TiCoO<sub>3</sub>, *physica status solidi (b)* **134**, 297 (1986).
- [26] Y. Lin, Y. Chang, W. Yang, and B. Tsai, Synthesis and characterization of ilmenite NiTiO<sub>3</sub> and CoTiO<sub>3</sub> prepared by a modified pechini method, *Journal of non-crystalline solids* **352**, 789 (2006).
- [27] S. Toth, B. Lake, *et al.*, 120 helical magnetic order in the distorted triangular antiferromagnet  $\alpha$ -CaCr<sub>2</sub>O<sub>4</sub>, *Physical Review B* **84**, 054452 (2011).
- [28] T. Adams, D. Sinclair, and A. West, Influence of processing conditions on the electrical properties of CaCu<sub>3</sub>Ti<sub>4</sub>O<sub>12</sub> ceramics, *Journal of the American Ceramic Society* **89**, 3129 (2006).
- [29] M. Subramanian, D. Li, N. Duan, B. Reisner, and A. Sleight, High dielectric constant in ACu<sub>3</sub>Ti<sub>4</sub>O<sub>12</sub> and ACu<sub>3</sub>Ti<sub>3</sub>FeO<sub>12</sub> phases, *Journal of Solid State Chemistry* **151**, 323 (2000).
- [30] Y. Kim, S. Wakimoto, S. Shapiro, P. Gehring, and A. Ramirez, Neutron scattering study of antiferromagnetic order in CaCu<sub>3</sub>Ti<sub>4</sub>O<sub>12</sub>, *Solid state communications* **121**, 625 (2002).

- [31] M. Wintenberger, G. André, and M. Gardette, Magnetic properties of green diopside  $\text{CuSiO}_3\text{H}_2\text{O}$  and of black diopside  $\text{CuSiO}_3$ , and magnetic structure of black diopside, *Solid state communications* **87**, 309 (1993).
- [32] T. Takayama and A. o. Kato, Hyperhoneycomb iridate  $\beta\text{-Li}_2\text{IrO}_3$  as a platform for Kitaev magnetism, *Physical review letters* **114**, 077202 (2015).
- [33] S. Pan, J. P. Smit, *et al.*, Synthesis, crystal structure, and nonlinear optical properties of  $\text{Bi}_2\text{Cu}_5\text{B}_4\text{O}_{14}$ , *Journal of Solid State Chemistry* **181**, 2087 (2008).
- [34] U. Arjun, V. Ramakrishnan, and R. Nath, Structural and magnetic properties of spin-1/2 layered ferrimagnet  $\text{Bi}_2\text{Cu}_5\text{B}_4\text{O}_{14}$ , *Journal of Alloys and Compounds* **683**, 205 (2016).
- [35] A. Austin, High pressure transformations of transition metal difluorides, *Journal of Physics and Chemistry of Solids* **30**, 1282 (1969).
- [36] A. Cooke, K. Gehring, and R. Lazenby, The magnetic properties of  $\text{NiF}_2$ , *Proceedings of the Physical Society (1958-1967)* **85**, 967 (1965).
- [37] D. C. Johnston, H. Prakash, W. H. Zachariasen, and R. Viswanathan, High temperature superconductivity in the Li-Ti-O ternary system, *Materials Research Bulletin* **8**, 777 (1973).
- [38] A. Kumatani *et al.*, Growth processes of lithium titanate thin films deposited by using pulsed laser deposition, *Applied Physics Letters* **101**, 123103 (2012).
- [39] P. Bityutskij and V. Khitrova, Electron diffraction investigation into crystal structures of anhydrous nickelates of alkaline earth elements (Ca, Sr, Ba), *Kristallografiya* **29**, 450 (1984).
- [40] J. Sannigrahi, J. Sichelschmidt, *et al.*, Microscopic investigation of low dimensional magnet  $\text{Sc}_2\text{Cu}_2\text{O}_5$ : combined experimental and ab initio approach, *Journal of Physics: Condensed Matter* **31**, 245802 (2019).
- [41] C. Emeis, F. Reinders, and E. Drent, Far-infrared investigation of the phase transition at 217 K in layer-structured  $\text{TiCl}_3$ , *Solid State Communications* **16**, 239 (1975).
- [42] J. He, S. Ma, P. Lyu, and P. Nachtigall, Unusual dirac half-metallicity with intrinsic ferromagnetism in vanadium trihalide monolayers, *Journal of Materials Chemistry C* **4**, 2518 (2016).
- [43] U. Troitzsch, A. G. Christy, A. C. Willis, and D. J. Ellis, Synthesis and crystal structure of  $\text{CuZrTiO}_5$  - a new crystal structure type, *Journal of Solid State Chemistry* **183**, 668 (2010).
- [44] H. Alyahyaei, R. Jishi, D. Guzman, O. Ta, and A. Sharif, Magnetic properties of  $\text{CuZrTiO}_5$ , in *APS March Meeting Abstracts*, Vol. 2011 (2011) pp. K1-053.
- [45] H.-M. Schwunck, P. Moser, and W. Jung, Das kupfer (II)-indium-oxidphosphat  $\text{CuInOPO}_4$  mit  $\alpha\text{-Fe}_2\text{OPO}_4$ -struktur, dargestellt durch die oxidation einer Cu/In/P-legierung im sauerstoffstrom, *Zeitschrift für anorganische und allgemeine Chemie* **625**, 407 (1999).
- [46] F. Sapina, J. Rodriguez-Carvajal, *et al.*, Crystal and magnetic structure of  $\text{Li}_2\text{CuO}_2$ , *Solid state communications* **74**, 779 (1990).
- [47] J. Hauck, K. Bickmann, *et al.*, Phase relations and physical properties of  $\text{Li}_{2-r}\text{Mg}_{1-r}\text{Cu}_{2-r}\text{O}_{3-r+x}$ , *Journal of Physics: Condensed Matter* **1**, 611 (1989).
- [48] S. Ebisu, T. Komatsu, *et al.*, Extremely large short-range order in an antiferromagnet  $\text{Li}_2\text{CuO}_2$ , *Journal of Physics and Chemistry of Solids* **59**, 1407 (1998).
- [49] A. Sologubenko, H. Ott, G. Dhalenne, and A. Revcolevschi, Universal behavior of spin-mediated energy transport in  $S=1/2$  chain cuprates:  $\text{BaCu}_2\text{Si}_2\text{O}_7$  as an example, *EPL (Europhysics Letters)* **62**, 540 (2003).
- [50] Y. Chen, Y. Zhang, and S. Feng, Hydrothermal synthesis and properties of pigments chinese purple  $\text{BaCuSi}_2\text{O}_6$  and dark blue  $\text{BaCu}_2\text{Si}_2\text{O}_7$ , *Dyes and Pigments* **105**, 167 (2014).
- [51] S. V. Berger, The crystal structure of cobaltpyroborate, *Acta Chem. Scand* **4**, 1054 (1950).
- [52] N. Kazak, N. Belskaya, *et al.*, Spin-flop transition in  $\text{Co}_2\text{B}_2\text{O}_5$  pyroborate, *JETP Letters* **114**, 92 (2021).
- [53] M. Zöller, E. Tillmanns, and G. Hentschel, Liebauite,  $\text{Ca}_3\text{Cu}_5\text{Si}_9\text{O}_{26}$  - A new silicate mineral with 14er single chain, *Zeitschrift für Kristallographie-Crystalline Materials* **200**, 115 (1992).
- [54] H. Witteveen and J. Van Veen, Magnetic susceptibilities of polycrystalline samples of the compounds  $\text{ANiCl}_3$  (A= Rb,  $\text{NH}_4$ , Tl, Cs) and  $\text{ANiBr}_3$  (A= Rb, Cs), *Journal of Physics and Chemistry of Solids* **35**, 337 (1974).
- [55] A. D. Raw, J. A. Ibers, and K. R. Poeppelmeier, Syntheses and structure of hydrothermally prepared  $\text{CsNiX}_3$  (X= Cl, Br, I), *Journal of Solid State Chemistry* **192**, 34 (2012).
- [56] Y. Sasago, M. Hase, *et al.*, Discovery of a spin-singlet ground state with an energy gap in  $\text{CaCuGe}_2\text{O}_6$ , *Physical Review B* **52**, 3533 (1995).
- [57] H.-J. Koo, D. Dai, and M.-H. Whangbo, Importance of supersuperexchange interactions in determining the dimensionality of magnetic properties. determination of strongly interacting spin exchange paths in  $\text{A}_2\text{Cu}(\text{PO}_4)_2$  (A= Ba, Sr),  $\text{ACuP}_2\text{O}_7$  (Ba, Ca, Sr, Pb),  $\text{CaCuGe}_2\text{O}_6$ , and  $\text{Cu}_2\text{UO}_2(\text{PO}_4)_2$  on the basis of qualitative spin dimer analysis, *Inorganic chemistry* **44**, 4359 (2005).
- [58] G. J. Redhammer, G. Tippelt, *et al.*, Structure of the clinopyroxene-type compound  $\text{CaCuGe}_2\text{O}_6$  between 15 and 800 K, *Acta Crystallographica Section B Structural Science* **61**, 367 (2005).
- [59] G. Giester and E. Libowitzky, Crystal structures and Raman spectra of  $\text{Cu}(\text{OH})\text{F}$  and  $\text{Cu}_3(\text{OH})_2\text{F}_4$ , *Zeitschrift für Kristallographie-Crystalline Materials* **218**, 351 (2003).
- [60] I. Danilovich, A. Merkulova, *et al.*, Vehement competition of multiple superexchange interactions and peculiar magnetically disordered state in  $\text{Cu}(\text{OH})\text{F}$ , *Journal of the Physical Society of Japan* **85**, 024709 (2016).
- [61] M. Bronold, C. Pettenkofer, and W. Jaegermann, Alkali metal intercalation into  $\text{SnS}_2$ , *Applied Physics A* **52**, 171 (1991).
- [62] G. Carter and D. Templeton, Polymorphism of sodium superoxide, *Journal of the American Chemical Society* **75**, 5247 (1953).

- [63] J. T. Sparks and T. Komoto, Magnetic properties of NaO<sub>2</sub> and KO<sub>2</sub>, *Journal of Applied Physics* **37**, 1040 (1966).
- [64] S. Desgreniers, Y. K. Vohra, and A. L. Ruoff, Optical response of very high density solid oxygen to 132 GPa, *Journal of Physical Chemistry* **94**, 1117 (1990).
- [65] K. Shimizu, K. Suhara, M. Ikumo, M. Eremets, and K. Amaya, Superconductivity in oxygen, *Nature* **393**, 767 (1998).
- [66] J. Winterlik, G. H. Fecher, *et al.*, Challenge of magnetism in strongly correlated open-shell 2p systems, *Physical review letters* **102**, 016401 (2009).
- [67] J. Winterlik, G. H. Fecher, *et al.*, Exotic magnetism in the alkali sesquioxides Rb<sub>4</sub>O<sub>6</sub> and Cs<sub>4</sub>O<sub>6</sub>, *Physical review B* **79**, 214410 (2009).
- [68] L. Andrews, Infrared spectrum, structure, vibrational potential function, and bonding in the lithium superoxide molecule LiO<sub>2</sub>, *The Journal of Chemical Physics* **50**, 4288 (1969).
- [69] H. Smith, R. Nicklow, L. Raubenheimer, and M. Wilkinson, Antiferromagnetism in potassium superoxide KO<sub>2</sub>, *Journal of Applied Physics* **37**, 1047 (1966).
- [70] J. Bertrand and D. Carpenter, Structure of K<sub>2</sub>BaCo(NO<sub>2</sub>)<sub>6</sub>, *Inorganic Chemistry* **5**, 514 (1966).
- [71] J. Bertrand, D. t. Carpenter, and A. Kalyanaraman, The structure of K<sub>2</sub>BaCo(NO<sub>2</sub>)<sub>6</sub> at 233 K: a static Jahn-Teller distortion, *Inorganica Chimica Acta* **5**, 113 (1971).
- [72] Y. Morioka and I. Nakagawa, Far-infrared spectra of K<sub>2</sub>MM'(NO<sub>2</sub>)<sub>6</sub> (M: Pb and Ba; M': Cu and Co): effect of dynamical distortion, *Spectrochimica Acta Part A: Molecular Spectroscopy* **37**, 437 (1981).
- [73] M. Sugantha, U. Varadaraju, and G. S. Rao, Synthesis and characterization of NZP phases, AM<sup>3+</sup>M<sup>4+</sup>P<sub>3</sub>O<sub>12</sub>, *Journal of solid state chemistry* **111**, 33 (1994).
- [74] H. Henke, The significance of the Jahn-Teller effect for the phase transitions of K<sub>2</sub>NbCl<sub>6</sub> and Rb<sub>2</sub>NbCl<sub>6</sub>, *Zeitschrift für Kristallographie* **222**, 477 (2007).
- [75] C. Authors and editors of the volumes III/17E-17F-41C, NaSb, KSb, RbSb, CsSb semiconducting properties, *Non-Tetrahedrally Bonded Elements and Binary Compounds I*, 1 (1998).
- [76] L. Jongen and G. Meyer, Dipotassium hexachlorotantalate (IV), K<sub>2</sub>TaCl<sub>6</sub>, *Acta Crystallographica Section E: Structure Reports Online* **60**, i91 (2004).
- [77] H. Ishikawa, T. Takayama, *et al.*, Ordering of hidden multipoles in spin-orbit entangled 5d<sup>1</sup> Ta chlorides, *Physical Review B* **100**, 045142 (2019).
- [78] K. M. Mogare, W. Klein, E. M. Peters, and M. Jansen, K<sub>3</sub>Na(RuO<sub>4</sub>)<sub>2</sub> and Rb<sub>3</sub>Na(RuO<sub>4</sub>)<sub>2</sub>, two new ruthenates with glaserite structure, *Solid state sciences* **8**, 500 (2006).
- [79] J. K. Burdett, S. A. Gramsch, and B. T. Schilf, A charge-stabilized Jahn-Teller distortion of the mixed valence system NaBa<sub>2</sub>Cu<sub>3</sub>O<sub>6</sub>, *Zeitschrift für anorganische und allgemeine Chemie* **621**, 1508 (1995).
- [80] M. Viola, M. Martínez-Lope, *et al.*, Structure and magnetic properties of Sr<sub>2</sub>CoWO<sub>6</sub>: an ordered double perovskite containing Co<sup>2+</sup>(HS) with unquenched orbital magnetic moment, *Chemistry of materials* **15**, 1655 (2003).
- [81] J. Longo and R. Ward, Magnetic compounds of hexavalent rhenium with the perovskite-type structure, *Journal of the American Chemical Society* **83**, 2816 (1961).
- [82] A. Sleight and J. Weiher, Magnetic and electrical properties of Ba<sub>2</sub>MReO<sub>6</sub> ordered perovskites, *Journal of Physics and Chemistry of Solids* **33**, 679 (1972).
- [83] C. A. Marjerrison, C. Mauws, *et al.*, Structure and magnetic properties of KRuO<sub>4</sub>, *Inorganic chemistry* **55**, 12897 (2016).
- [84] J. R. Günter, The crystal structure of topotactically dehydrated copper (II) formate tetrahydrate, *Journal of Solid State Chemistry* **35**, 43 (1980).
- [85] T. Castner and M. Seehra, Critical behavior of the electron-paramagnetic-resonance linewidth of a spin-1/2 two-dimensional antiferromagnet, *Physical Review B* **47**, 578 (1993).
- [86] R. W. Smith and D. A. Keszler, Synthesis, structure, and properties of the orthoborate SrCu<sub>2</sub>(BO<sub>3</sub>)<sub>2</sub>, *Journal of Solid State Chemistry* **93**, 430 (1991).
- [87] G. Liu, J. Luo, *et al.*, In-plane substitution effect on the magnetic properties of the two-dimensional spin-gap system SrCu<sub>2</sub>(BO<sub>3</sub>)<sub>2</sub>, *Physical Review B* **73**, 014414 (2006).
- [88] R. Becker and H. Berger, Reinvestigation of CuSe<sub>2</sub>O<sub>5</sub>, *Acta Crystallographica Section E: Structure Reports Online* **62**, i256 (2006).
- [89] C. Khattak, J. Hurst, and D. Cox, Crystal growth, and electrical and magnetic properties of Ba<sub>2</sub>CoWO<sub>6</sub>, *Materials Research Bulletin* **10**, 1343 (1975).



